ELSEVIER

Contents lists available at ScienceDirect

Additive Manufacturing

journal homepage: www.elsevier.com/locate/addma



Research paper

Pressure-assisted binder jet additive manufacturing of solid propellants

Levi Kirby ^a, Adam Lawrence ^b, H.S. Udaykumar ^c, Travis Sippel ^b, Xuan Song ^{a,c,*}

- ^a Department of Industrial and Systems Engineering, The University of Iowa, USA
- ^b Department of Mechanical Engineering, Iowa State University, USA
- ^c Department of Mechanical Engineering, The University of Iowa, USA

ARTICLE INFO

Keywords: Solid propellant Binder jet Solids loading Density Burn rate

ABSTRACT

Solid propellants are used as an energy source in many applications such as space launch, tactical, and gun propulsion. In traditional fabrication methods, solid propellants are cast or extruded into cylindrical mandrels. The resulting propellants are highly dense, durable, and have uniform composition. These characteristics provide consistent and reliable thrust, but do not provide a way to throttle or alter the thrust profile once ignited. Additive manufacturing (AM) holds the promise of facilitating precise control over thrust and propulsion by spatially manipulating the macro- and micro-structures of a solid propellant. However, this advantage is often accompanied by trade-offs in other crucial characteristics, including solids loading, density, mechanical properties, and consequently burning performance. Here, we report, for the first time, the use of a pressure-assisted binder jetting (PBJ) AM process to manufacture solid propellant materials. The PBJ process shows great promise in the fabrication of highly resolute propellants with high solids loading, sufficient density, and sufficient mechanical properties. Particular emphasis is given to the effects of process parameters including applied pressure and step-over on the density and solids loading (up to 85.5% and 96.1%, respectively) of printed propellants. Mechanical properties of printed propellants are analyzed and compared with those achieved by other traditional fabrication and AM methods. The results demonstrate that our method can fabricate propellants with sufficient tensile strength, elongation, and E-modulus (up to 0.88 MPa, 9.1%, and 20.7 MPa, respectively). Solid propellants with complex grain geometries and changeable burn rates (e.g., variations of 90%) were printed to showcase the capability of the PBJ process in tuning the burning behaviors of propellants in situ.

1. Introduction

Solid propellants are mixtures containing both fuel and oxidizer components, and are widely used to provide simple, reliable, high performance thrust for propulsion applications such as space launch, tactical, and small arms. Upon ignition, the fuel and oxidizer particles in a solid propellant burn to hot gaseous products which are expelled out of the combustion chamber, generating thrust for the rocket, missile, or ammunition [1]. The burning behavior of a solid propellant is dependent on the macro-structure (e.g., grain geometry) and micro-structure (e.g., chemical composition, solids loading, particle size, density) of the material [2–5]. Specifically, propellant grain geometry can determine the burning surface and thrust history [4], while solids loading and density can significantly influence the burn rates [3,5]. Accurate spatial control of the macro- and micro-structures of a solid propellant offers the potential to enable highly tunable thrust and propulsion [6]. However, traditional manufacturing techniques, such as casting, lack the

flexibility to spatially control the macro- and micro-structures of a solid propellant [7].

Alternatively, research in recent years has steered toward the use of additive manufacturing (AM) processes to fabricate solid propellants. AM processes, such as extrusion-based methods and stereolithography, can achieve complex grain geometries, but often at the cost of other crucial characteristics, including solids loading, density, and mechanical properties. For example, extrusion-based methods typically require relatively low solids loading (under 85%) and large nozzle sizes (~500 µm) [8] to ensure slurry extrudability, which ultimately lead to poor printing resolution [4] and lower performing propellants [9]. In order to achieve higher solids loading and higher burning performance, Gunduz and co-workers have developed and demonstrated a ultrasonic vibration-assisted (VAP) printing process [10]. In this technique, extrusion is achieved by using a combination of both gas pressurization of the propellant-filled print reservoir and a localized lowering of propellant viscosity through ultrasonic vibration of the print nozzle. Using

^{*} Corresponding author at: Department of Industrial and Systems Engineering, The University of Iowa, USA. *E-mail address:* xuan-song@uiowa.edu (X. Song).

this technique, the authors were able to print up to 80 wt% solids aluminized composite solid propellants with a ultraviolet (UV) curable epoxy binder [10]. Solids loadings of up to 85 wt% have also been achieved in separate studies when using hydroxyl-terminated polybutadiene (HTPB) as the binder [11]. In comparison to extrusion-based methods, stereolithography can fabricate solid propellants with higher

resolutions based on a photocurable fuel-oxidizer slurry, but the process is constrained by viscosity, therefore, dropping the solids loading of the printed propellants to levels lower than other manufacturing techniques [12,13].

This paper aims to establish a pressure-assisted binder jetting (PBJ) process to fabricate highly resolute propellants with high solids loading,

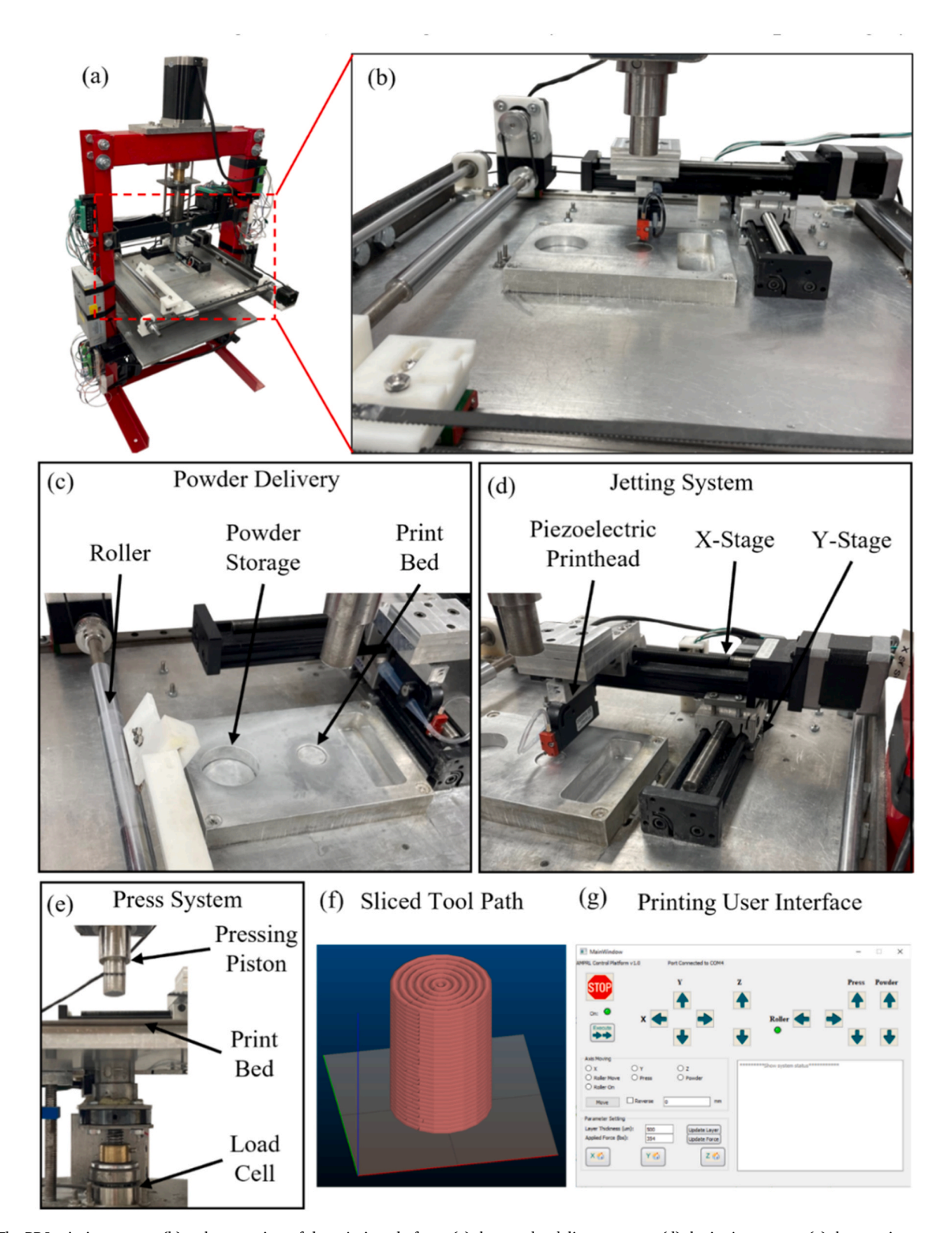


Fig. 1. The PBJ printing system; (b) a close-up view of the printing platform; (c) the powder delivery system; (d) the jetting system; (e) the pressing system; (f) the sliced tool path: and (g) the printing user interface.

sufficient density, and sufficient mechanical properties. To the authors' knowledge, this is the first report of efforts to additively manufacture a granular composite energetic material using a binder jetting process. Through integrating a layerwise pressing mechanism, our PBJ process has the potential to provide a printing resolution comparable to stereolithography [14-17] and enable maximized densification of the propellant that can meet or exceed that of propellants fabricated by extrusion-based AM methods. In this work, ammonium perchlorate (AP) was used as the oxidizer, one of the most commonly used due to its density, thermal stability, and higher proportion of oxygen [18]; HTPB was selected as the fuel binder due to its ease of curing at a lower temperature, reproducibility, good mechanical properties over a wider temperature range, and better ageing properties [18]. Through alteration of different process parameters such as applied pressure and step-over, this study will also highlight the feasibility of reliably manufacturing tunable solid propellants with the PBJ printing method.

2. Methods

2.1. Pressure-assisted binder jetting

An in-house designed and constructed PBJ printer is shown in Fig. 1a and b. The PBJ printer is primarily comprised of a powder delivery system (Fig. 1c), a piezoelectric jetting system (Fig. 1d), and a pressing system (Fig. 1e). In the manufacturing of a propellant layer, the powder delivery system (Fig. 1c) spreads a thin layer of oxidizer particles (e.g., AP) on top of a print bed via a counter-clockwise rotating roller mechanism. The roller traverses back and forth to transfer the oxidizer particles from a powder storage reservoir onto the print bed. The print bed is driven by a Nema 23 step motor to ensure precise control of layer thickness. The piezoelectric jetting system utilizes a PipeJet nanodispenser (Biofluidix GMbH, Freiburg, Germany) to deposit binder droplets into the print bed, as shown in Fig. 1d. The system offers a range of nozzle diameters to accommodate different resolution and binder viscosity requirements. In this study, we selected the 500-micron nozzle size for printing. The jettability of binder was analyzed using a smart drop imaging system, as shown in Fig. 3a. The camera captures the images of each droplet as it is deposited to characterize the droplet shape and volume. The Pipejet nanodispenser is attached to two perpendicular linear stages (X-Slide, Velmex, Bloomfield, NY; Fig. 1b) serving as the xy movement. The pressing system is housed in a 12-ton hydraulic press frame. A piston is mounted on top of the frame and is driven up and down in the z-direction by a motorized lead screw to apply a uniaxial pressure on the print bed. Under the print bed lies a 5 K load cell (THC-5 K-V, Transducer Techniques, Temecula, CA) to determine the force being applied to the print bed, allowing for precise control of the applied pressure. The PBJ system is controlled by an Arduino Mega microcontroller and an in-house-developed control software (Fig. 1 g). Slic3r software (slic3r.org) was used to generate G-code from a given computer-aided design (CAD) model based on selected printing parameters, e.g., layer thickness and step-over, which is then used to control the PBJ system to print a propellant (Fig. 1 f). In this study, the print bed size is set at 20 mm in diameter for proof-of-concept purposes. The process can be readily scaled up when transitioning to production standards.

2.2. Printing process

The printing procedure for the PBJ process is highlighted in Fig. 2a. Step 1: To start, the powder storage raises, and the print bed lowers from its zero location to the specified layer thickness. Step 2: Then, the roller rotates counterclockwise and moves laterally to deposit a thin, uniform layer of AP particles from the powder storage to the print bed. Any excess powder is transferred to a surplus location. Step 3: Once spread, the pressing piston applies a selected force to the print bed, increasing the density of the powder. Step 4: The PipeJet nanodispenser follows the

created G-code to deposit droplets of binder in the tool-path pattern of the sliced layer. A denser pattern provides more binder for the particles, which alters both the mechanical properties and fuel-to-oxidizer ratio of the final propellants. Step 5: The cycle repeats until all sliced layers have been printed.

The uniqueness of the PBJ process comes in the ability to control its macro-scale geometry without sacrificing the micro-structures (including solids loading and density) and physical properties of a solid propellant. Meanwhile, the PBJ process can strategically alter the applied pressure and step-over for each layer to tune the solids loading (via varying binder addition) and density of a propellant, achieving gradients in porosity, oxidizer-to-fuel contact, and thereby spatially controlled burning behaviors [19]. Throughout the remainder of the paper, the term "applied pressure" refers to the pressure experienced by the powder in the die as a result of the press. As shown in Fig. 2b and c, an applied pressure significantly influences the powder packing density of a printed layer, and the step-over distance controls the amount of binder being deposited and the local equivalence ratio.

2.3. Materials

A 90-micron AP powder was used as-received from Pyro Chemical Source (Hayward, MN, USA) without further modification. A HTPB binder solution was formulated from a mixture of an HTPB monomer (R45M, RCS), a curative (isophorone diisocyanate or IPDI from Sigma Aldrich), a tepanol bonding agent (HX-752, RCS), a plasticizer (isodecyl pelargonate or IDP, RCS), and a hexane diluent solvent (Sigma Aldrich). This formulation (excluding the hexane diluent) has been extensively utilized as the binder in our previous work [20-22] for creating cast solid propellants. The tepanol bonding agent was added to enhance the bonding strength between AP particles and the binder after curing. The hexane diluent solvent was used to reduce the viscosity and surface tension of the binder solution so as to improve the jettability of the binder via the Pipejet nanodispenser. Hexane was chosen because it is miscible in the R45 monomer, has a high evaporation rate to facilitate solvent removal, and does not adversely affect the R45 crosslinking process. In this study, we chose to use a monomodal powder without any additives (e.g., Aluminum powder) to facilitate the understanding of the fundamental capabilities of the proposed PBJ process before delving into system or material optimization.

The optimized binder formulation is given in Fig. 3b, which can ensure sufficient droplet jettability and thermal curability. Fig. 3a indicates that this formulation can achieve desired spherical droplets (Fig. 3a-iv) as opposed to other formulations (e.g., 20% hexane in Fig. 3a-i, 40% hexane in Fig. 3a-ii, no hexane in Fig. 3a-iii). Tests were also done to determine the hexane loss during curing to determine the final binder composition. Samples of 5 g HTPB, 10 g HTPB, 50 g HTPB, 90 wt% 90-micron AP in HTPB, and 90 wt% 200-micron AP in HTPB were weighed before and after curing at 60 °C for 1 week. The difference in weight was compared with the initial amount of hexane placed in the samples. The hexane losses measured for different AP particle sizes and solids loading (Fig. 3c) were relatively constant at 32% which was then used in calculations for the density and solids loading of printed propellants.

2.4. Study of solids loading and density

The effects of different processing parameters on solids loading and density are studied by examining the global solids loading and density of specimens fabricated under different sets of printing parameters, including applied pressure (0 MPa, 5 MPa, and 10 MPa) and step-over (0.65 mm, 0.7 mm, 0.8 mm, and 0.89 mm). A cylindrical shape of 8 mm in diameter and 18 mm in length was used for all samples. The layer thickness prior to pressing was kept at 500 μm . The solids loading of a printed shape was determined using Eq. (1).

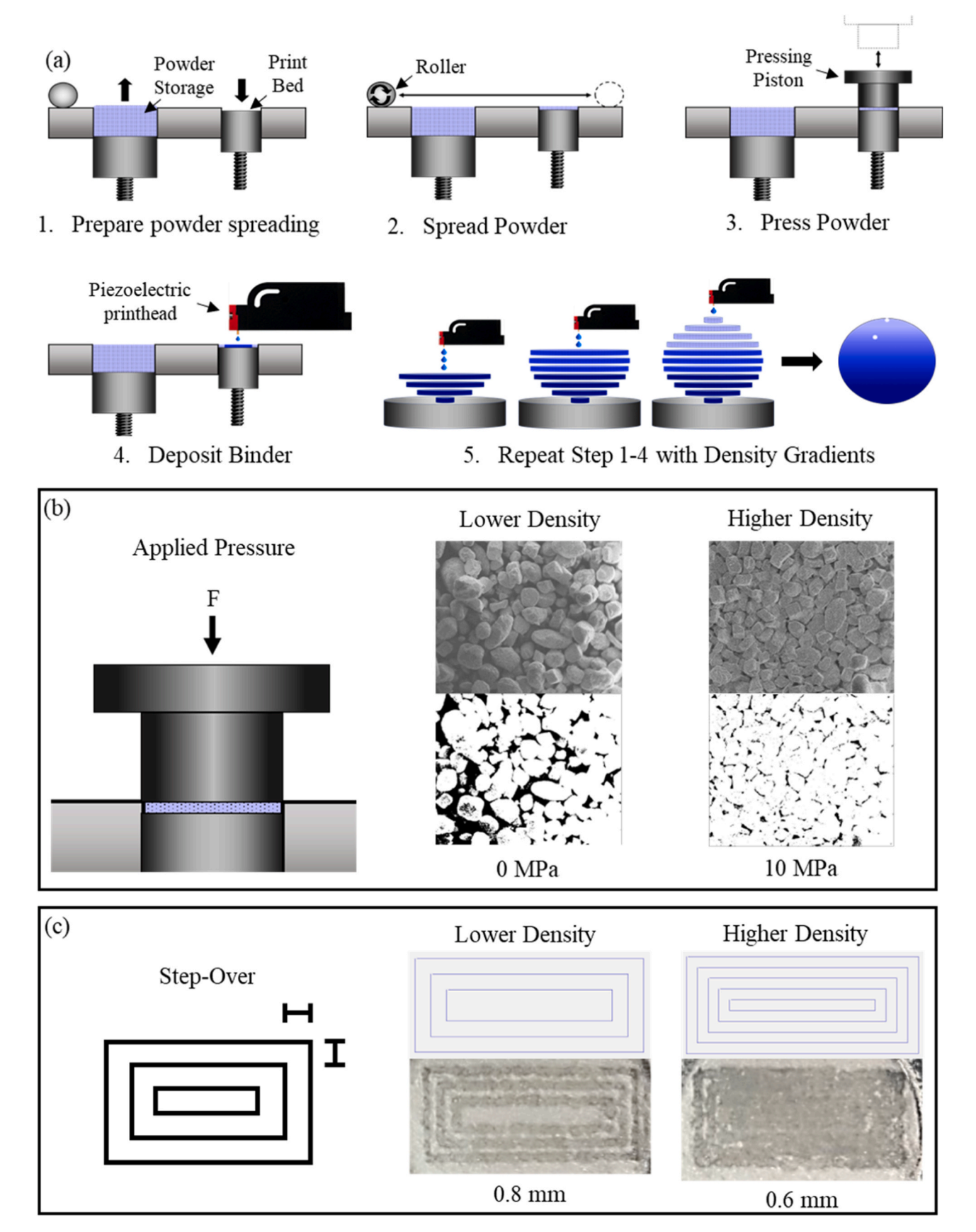


Fig. 2. (a) Printing schematic demonstrating the process; controllable parameters of interest, including (b) applied pressure and (c) step-ver.

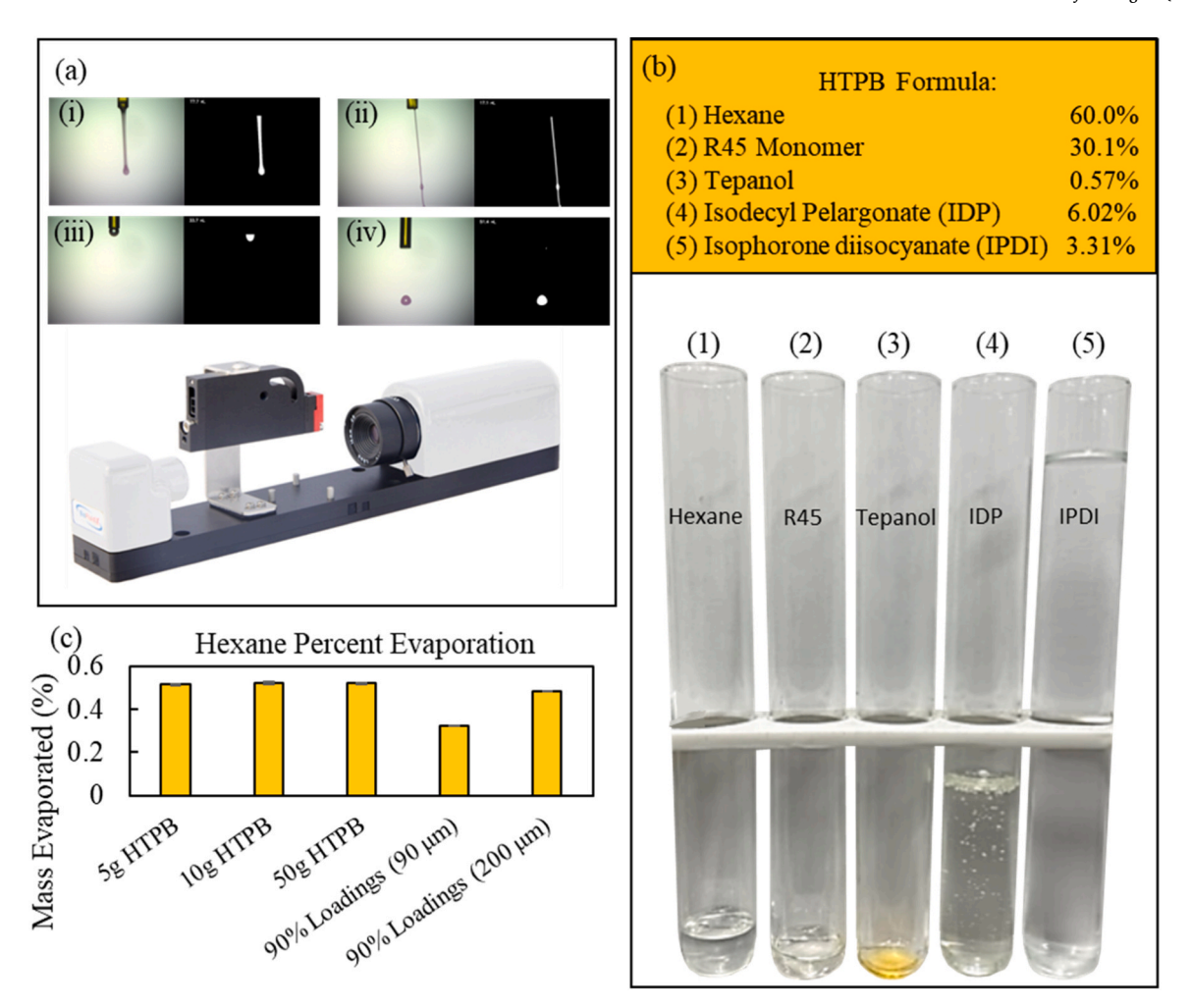


Fig. 3. (a) Jettabiltiy of different binder formulations; (b) the optimized binder formula used (in weight percentage); and (c) evaporation measurements for hexane.

Solids Loading =
$$\frac{m_p}{m_p + m_b} * 100\%$$
 (1)

where m_b is the mass of binders deposited in a printed shape, and m_p is the mass of AP particles in a printed shape. m_b was determined from the number of droplets used in the printing and the droplet volume measured from the integrated optical imaging system (Fig. 3a). m_p was estimated from the powder bed density ρ_{pb} and the volume of the printed shape V_{print} , shown in Eq. (2):

$$m_p = \rho_{pb} \bullet V_{print} \tag{2}$$

The powder bed densities ρ_{pb} were determined by measuring the mass and volume of five layers of AP particles after layerwise pressing, as given by Eq. (3).

$$\rho_{pb} = \frac{m_{pb}}{V_{pb}} \tag{3}$$

The absolute density ρ of the printed part was calculated using Eq. (4).

$$\rho = (VF_p * \rho_{AP}) + (VF_b * \rho_b) \tag{4}$$

where VF_p and VF_b are the volume fraction of the AP powder and the binder, respectively, ρ_{AP} is the density of the AP crystal ($\rho_{AP}=0.00195g/mm^3$), and ρ_b is the binder density. VF_p was calculated from the measured powder bed density using Eq. (5), and VF_b was calculated from the deposited volume of binder and the volume of the printed shape V_{print} using Eq. (6).

$$VF_p = \frac{\rho_{pb}}{\rho_{AP}} \tag{5}$$

$$VF_b = \frac{V_b}{V_{voist}} \tag{6}$$

The relative density ρ_{N} of the printed part was then calculated using Eq. (7) based on the theoretical maximum density (TMD), i.e., the density of the AP sample with pores that are fully saturated with binder.

$$\rho_{\%} = \left(\frac{\rho}{TMD} * 100\%\right) \tag{7}$$

2.5. Study of mechanical properties and microstructures

Mechanical properties of printed propellants were analyzed using a tensile tester (Test Resources, Shakopee, MN). Samples were printed per the ASTM D638 type IV standard cross-section with a thickness of 4 mm \pm 0.2 and a width of 8 mm \pm 0.2 [23]. Due to printing area restrictions, our sample lengths were decreased to 18 mm. One group of samples was printed using different step-overs including 0.6 mm, 0.7 mm, and 0.8 mm with inter-layer pressure kept constant at 0 MPa (no pressing). Another group of samples were printed with varying inter-layer pressures of 0 MPa, 2.5 MPa, 5 MPa, 7.5 MPa, and 10 MPa with step-over kept constant at 0.7 mm. Prior to the tensile testing, each printed sample was inserted and glued onto two plastic clamps, which were then clamped in the jaws of the tensile tester with sufficient force (Fig. 9a). The plastic clamps were designed to prevent damage to the propellant during sample clamping and were printed by fused deposition modeling

(FDM). The tensile testing was performed at a tensile rate of 6.35 mm/minute. Key mechanical properties, including tensile strength (σ_m) , E-modulus (E), and elongation (δ), were computed from the stress-strain curves of the tensile testing. The mechanical properties for each set of printing parameters were compared with those of propellants obtained by traditional fabrication methods. The surfaces (top and fracture) of printed specimens after tensile testing were examined using scanning electron microscopy (SEM) at 60X magnification for better understanding of the process-microstructure relationships.

2.6. Study of burning behaviors

The burn rate of the printed propellants at standard temperature and pressure (STP) was measured using a high-speed camera and a bridgewire ignition method, as displayed in Fig. 4. Samples were placed inside a burn chamber at room temperature. For ignition, a 20-gauge nickel-chromium (Ni-Cr) wire was crimped to provide a highresistance location for Ohmic heating and placed in contact with the surface of the propellant by connecting each wire end to a variable transformer (Variac, 120 VAC, 5 Amp input, 0-140 VAC output), which allows for controlled heating of the wire until ignition begins. Burning rates and burning surface evolution were captured using a high-speed camera (Phantom ir300, 14-bit depth, 500 Hz, 100 µs exposure) with a long-distance microscopic objective (Infinity, K2 Distamax). This setup provided a 27.3 \times 20.5 mm field of view (FOV) (800 \times 600 pixels²) with a scale of 29.3 pixels/mm. Burning rate and video post-processing was completed using ImageJ software. All burn rates reported were taken from the middle portion of the propellant strand burn to avoid transient phases of the burn (i.e., ignition and extinction).

3. Results and discussion

3.1. Test cases

Multiple test cases were printed to display the capabilities of the PBJ process, as shown in Fig. 5, including a chain, a spiral ornament, a spiral, a sea turtle, a colosseum, a Moai head, and a centrifugal fan. The samples were printed using AP powder and the HTPB binder formulation. The applied pressure was set as 10 MPa, and the step-over was set as 0.7 mm. The samples were cured in the lab oven at 60 °C for one week. The nozzle size used in the PipeJet nanodispenser is $\sim\!500~\mu\text{m}$. Of particular note is that the test prints hold their intended shape during densification, and there does not appear to be significant binder migration into binder-free regions that would deform final print shape during densification, highlighting the great potential of PBJ in generating highly resolute propellants. It is important to acknowledge that improper control of the pressure applied to each layer can result in detrimental impacts on the printing resolution due to binder diffusion as studied in our prior work

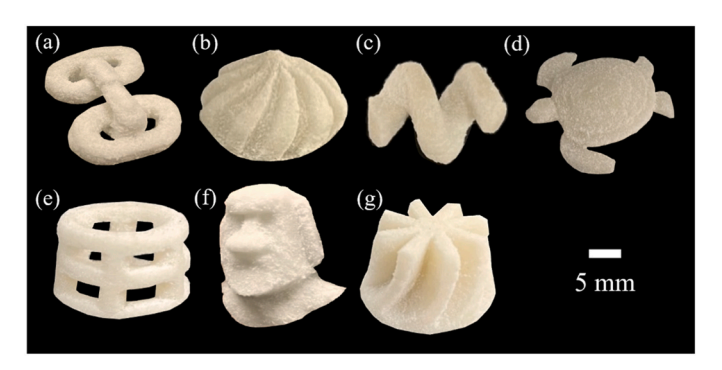


Fig. 5. Test cases printed by the PBJ process, including (a) a chain, (b) a spiral ornament, (c) a spiral, (d) a sea turtle, (e) a colosseum, (f) a Moai head, (g) and a centrifugal fan. Binder jetting nozzle size: \sim 500 μ m.

[24]. Nevertheless, our previous studies [24,25] have demonstrated the feasibility of mitigating such diffusion by strategically adjusting printing parameters, such as applied pressure level and droplet saturation level, according to the inherent compaction properties of the printed powder. Hence, there exists an opportunity for continued technological development to further refine the printing resolution of propellants using the PBJ process.

3.2. Solids loading and density

Fig. 6a illustrates the effects of applied pressure and step-over on the solids loading of printed propellants. When the applied pressure was raised from 0 MPa to 5 MPa, the solids loading increased by nearly 4%. As the applied pressure was further increased from 5 MPa to 10 MPa, the resulting increase in solids loading was minimal, with an increment of less than 0.5%. The increased applied pressure enables more powder to be packed in a fixed volume, consequently enhancing the maximum solids loading of printed propellants (i.e., in the case with no binder inclusion). However, once the applied pressure reached a certain threshold, further increases did not yield significant particle rearrangement, leading to a relatively constant maximum solids loading. While the applied pressure predominantly dictates the maximum solids loading of a printed propellant, the step-over parameter plays an additional role in fine-tuning solids loading by regulating the level of binder saturation within the pores. A reduced step-over results in a higher amount of binder being deposited within the same volume of powder, leading to a decrease in the solids loading. The PBJ process, because of its in-situ mixing of binder and granular solids during manufacture, is capable of producing composite structures with variable or compositionally graded solids loading through localized adjustment of binder flux per layer by changing the step-over parameter.

Applied pressure was found to have a greater impact on the density

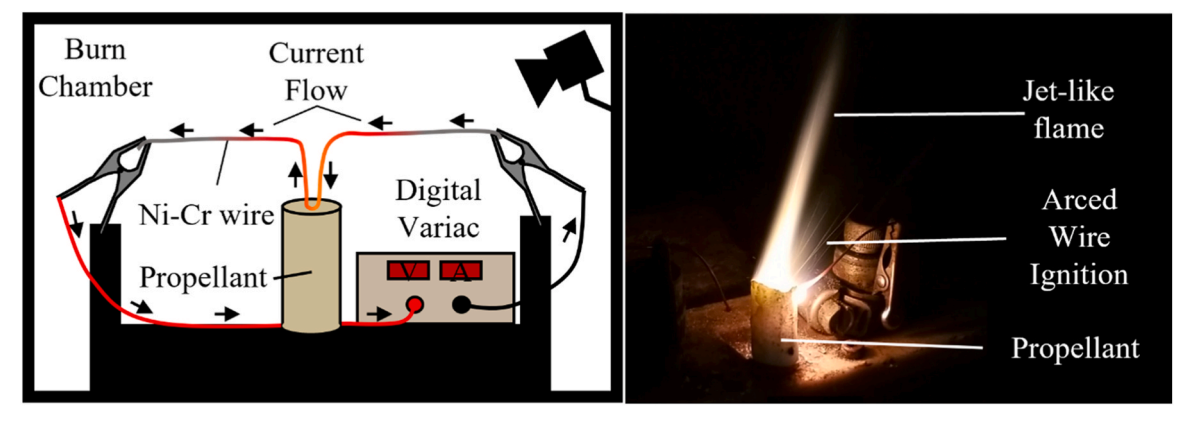


Fig. 4. Schematic of the burn rate setup with a display of a burning propellant.

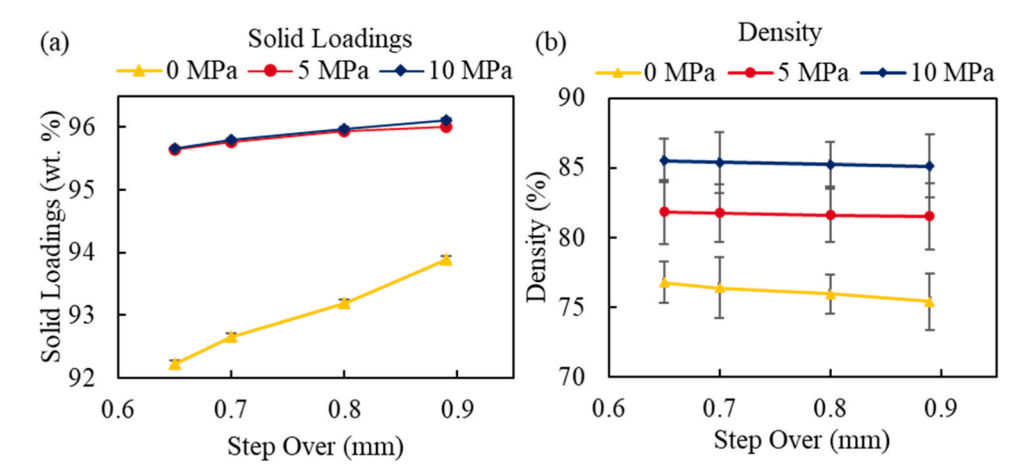


Fig. 6. Effects of step-over and applied pressure on (a) solids loading and (b) density. Data reported is averages of 3 measurements and scale bars indicate one standard deviation.

(Fig. 6b), while step-over exhibited a minor influence. An increase in pressure from 0 MPa to 5 MPa led to a 7.3% increase in the resulting density, and an increase from 5 MPa to 10 MPa resulted in a 4.5% increase. This impact can be attributed to a significant increase in powder bed density stemming from the application of a higher compaction force. On the other hand, as the step-over increased from 0.65 mm to 0.89 mm, the amount of binder deposited in the powder bed decreased. However, this decrease only caused a slight decline in density, in comparison to the substantial effect of applied pressure. The highest density was achieved at the highest pressure used, 10 MPa, and the lowest step-over, 0.65 mm.

Fig. 7 illustrates a comparison between the density and solids loading of propellants fabricated using the PBJ process and other propellant fabrication processes [3,4,26–30]. The solids loading achieved through our PBJ approach far exceeded that of existing methods, while the density achieved with PBJ surpassed that of most AM processes and was near comparable to traditional methods. It's worth noting that the highest density achieved in this study (85.5%) was lower than that achieved by certain extrusion-based processes [3,8], as illustrated in Fig. 7. However, we believe there remains considerable room for improvements to enhance the printed density. For example, our current fabrication process employs a monomodal powder distribution. Refining the feedstock powder with a bimodal or trimodal distribution holds the promise to promote the printed density. Moreover, the maximum compaction pressure applied in this work was restricted to 10 MPa due

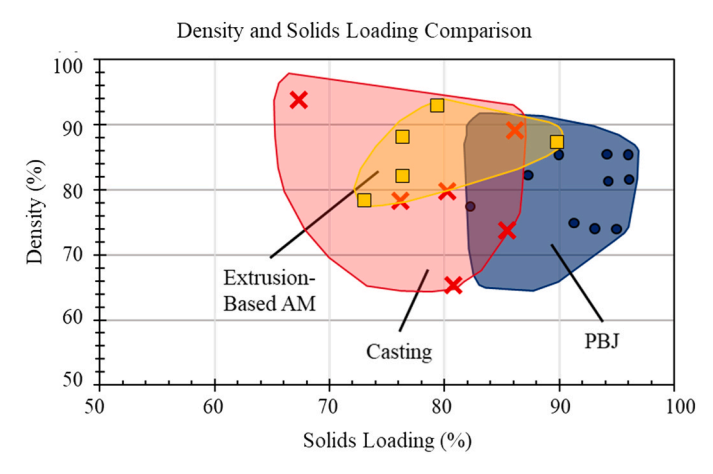


Fig. 7. Ashby plot for the estimated range of density and solids loading achievable through the PBJ process in comparison to other fabrication techniques [3,4,26-30].

to hardware limitations. An enhanced pressing system could likely enable higher density levels. Furthermore, a significant degree of porosity in the printed samples appeared to originate from the evaporation of the hexane in the binder during curing. Utilizing a binder with reduced hexane content can potentially minimize the formation of pores during the curing process. Collectively, these strategies provide a clear path towards enhancing the density capabilities of PBJ in the future.

Based on Eqs.(1)–(7), we established an empirical model to estimate the solids loading and density of propellants printed under different applied pressures (0–10 MPa) and step-overs (0.65–0.89 mm), as given in Eqs. (8) and (9), respectively.

Solids Loading_{model} =
$$\frac{V_{CAD} \bullet \rho_{pb}}{V_{CAD} \bullet \rho_{pb} + \rho_b \bullet DI \bullet V_{dep_binder}}$$
(8)

$$\rho_{model} = \rho_{pb} + (\frac{DI \bullet V_{dep_binder}}{V_{CAD}}) \bullet \rho_b$$
(9)

where V_{CAD} is the desired volume of a print, ρ_{pb} is the powder bed density, DI is the binder diffusion index, and V_{dep_binder} is the total volume of deposited binder. V_{CAD} is determined from the CAD model of a propellant, and all the other parameters are dependent on the applied pressure and step-over. Specifically, ρ_{pb} was experimentally identified as linear functions of applied pressure, as given in Eq. (10).

$$\rho_{pb} = f_{\rho_{pb}}(pressure) \tag{10}$$

Binder diffusion index DI is defined to estimate the diffusion of the binder in the powder bed under the applied pressure, which is calculated as the ratio between the desired volume V_{CAD} of a print and the actual volume of a print. It was experimentally fitted as a quadratic function of pressure and step-over, as depicted in Eq. (11).

$$DI = f_{DI}(pressure, step-over)$$
 (11)

The total volume V_{dep_binder} of deposited binder is correlated to applied pressure and step-over via Eq. (12):

$$V_{dep_binder} = \frac{k \bullet V_{CAD}}{step-over \bullet L_{V_{CAD}}}$$
 (12)

where k is a constant related to the inkjet system and can be estimated from experiments, $L_{V_{CAD}}$ is the number of layers required for printing a given part and has a linear relationship with the applied pressure, as given in Eq. (13):

$$L_{V_{CAD}} = f_{L_{V_{CAD}}}(pressure) \tag{13}$$

The prediction results from this model align well with the

experimental results for both applied pressure and step-over, as shown in Fig. 8. The minor discrepancy between the prediction and experimental result is likely caused by the simplification of the binder diffusion behaviors in a compacted powder bed (i.e., using the diffusion index DI). Further studies on binder diffusion in a compacted powder bed could reduce the discrepancy. Using these simple empirical models, we can reversely derive a set of printing parameters to achieve a target combination of solids loading and density for various applications of propellants.

3.3. Mechanical properties

Fig. 9a shows a printed specimen before and after tensile testing. The stress-strain curves of the printed specimens under different applied pressures (0, 5, and 10 MPa) and step-over (0.6, 0.7, and 0.8 mm) are shown in Fig. 9b and c, respectively. It can be seen that a higher pressure resulted in a material with greater stiffness, higher ultimate tensile strength, and lower ultimate tensile strain, while a higher step-over led to lower stiffness, lower ultimate tensile strength, and greater ultimate tensile strain. Both are attributed to the effects of applied pressure and step-over on the density of the specimens, as suggested by Fig. 8d. With that, a higher pressure or a lower step-over resulted in a higher density which increased the strength but reduced the ductility of the part. Based off the loading curves, a higher pressure and lower step-over are desired to maximize the propellant strength.

Fig. 9d-i show the effects of applied pressure and step-over on mechanical properties of printed propellants, including tensile strength, emodulus, and elongation. It was found that an increase in applied pressure from 0 to 10 MPa lead to a $\sim\!\!681\%$ increase in the tensile strength of the printed propellant, a $\sim\!\!1620\%$ increase in the E-modulus, and a $\sim\!\!55\%$ decrease in the elongation. The increasing stiffness of the printed parts can be caused by their lower porosity achieved by higher applied pressures.

As seen in Fig. 9g-i, an increasing step-over from 0.6 to 0.8 mm led to a \sim 47% decrease in the tensile strength, a \sim 79% decrease in the E-modulus, and a \sim 175% increase in the elongation at break. A higher

step-over contributed to much lower effective saturation ratios (refer to Fig. 10) in the printed parts, suggesting a reduced concentration of binder and a higher level of porosity. With the powder bed density remaining relatively constant across the step-overs, the reduced amount of binder in the powder bed yielded less connectivity between the particles, decreasing the strength of the propellant, and the increased number of pores promoted the elasticity of the propellant.

The mechanical properties of the specimens printed at different applied pressures were also compared with those of propellants fabricated by traditional manufacturing technologies, as shown in Fig. 9d-f [4,31–38]. The specimens printed at higher pressures (e.g., 7.5 or 10 MPa) exhibited higher tensile strengths than those made by traditional casting, extrusion, or AM approaches. Even though PBJ-printed specimens possessed lower elongation than traditional casting/extrusion specimens [39] (\sim 5% vs \sim 20% elongation), our E-modulus is comparable to casting/extrusion specimens and is more favorable than those of propellants achieved by existing AM processes [4,36].

3.4. Microstructures

Fig. 11 shows the SEM images for the parts printed under varying pressures and step-overs. The SEM images were taken from the top surface of a printed sample upon completion of printing. When no pressure (0 MPa) was applied during the printing, the samples had very apparent porosity with a rough surface (Fig. 11a, d, and g). The deep valleys, highlighted in red, formed under the larger step-over (i.e., 0.8 mm, Fig. 11g) resulted from a lack of binder in the areas, causing the particles to fall apart from the composite. Under no pressure, as the stepover decreased from 0.8 mm to 0.6 mm (Fig. 11g, d, and a), the deposited binder amount increased, and the valleys became less prevalent. As the applied pressure increased from 0 MPa to 10 MPa, the surface of the part became much more uniform owing to the consolidated powder bed density. A more compacted powder bed also had less pore space, highlighted in green, to be saturated by the binder, allowing the larger step-over (0.8 mm, Fig. 11i and 11ii) to create a sample with better uniformity and surface finish than those achieved under no

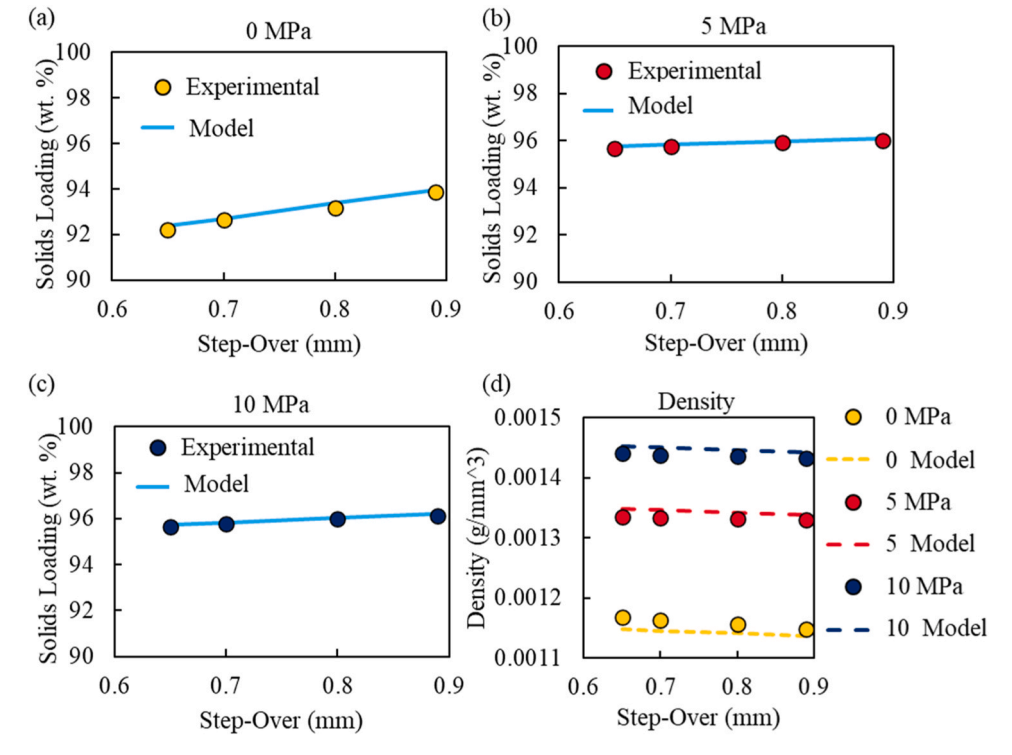


Fig. 8. Experimental and modeling results of (a)- (c) the solids loading and (d) density in relation to pressure and step-over.

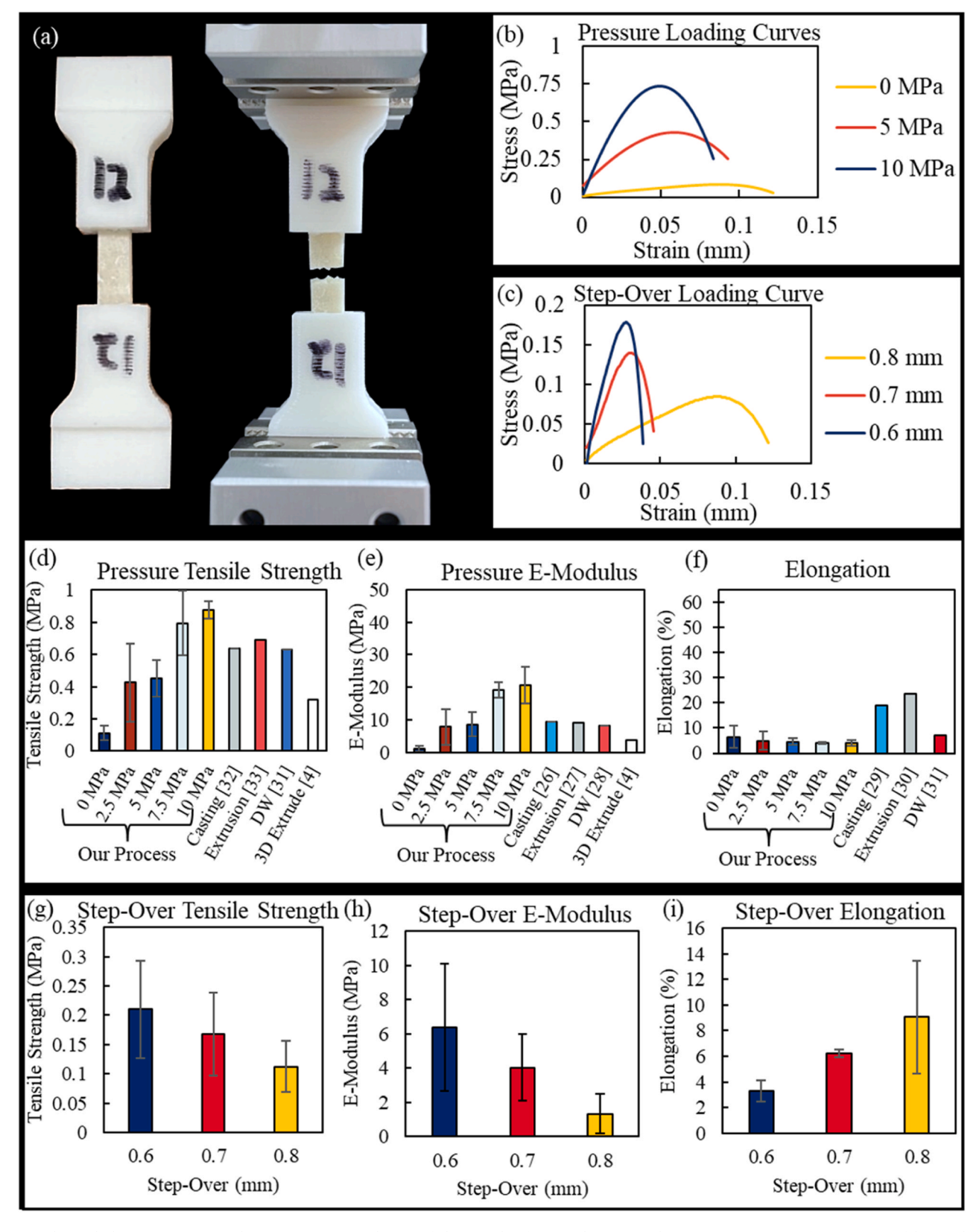


Fig. 9. Mechanical characterization results. (a) A specimen showing failure mode after tensile testing. (b) Stress-strain curves for specimens fabricated under different (b) applied pressures and (c) step-overs. (d) - (i) The mechanical properties of specimens fabricated under different applied pressures and step-overs. For (d)-(f), the step-over was fixed at 0.7 mm; for (g)-(i), the applied pressure was fixed at 0 MPa. The materials used in the literature include [4] 78% AP/HTPB, [31] 80% AP/Al/HTPB/TMB, [32] 82% AP/Al/HTPB, [33] 90% AP/NC/HTPB, [34] 85% AP/Al/HTPB, [35] 81% AP/Al/HTPB, [36] DW (Direct Write) - 80% NaCl/HTPB, [37] 86% AP/Al/HTPB, and [38] 80% AP/HTPB.

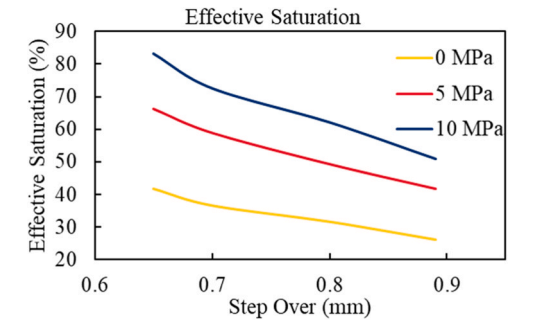


Fig. 10. Effective binder saturation level for 0 MPa, 5 MPa, and 10 MPa.

pressure. Under a smaller step-over (0.6 mm, Fig. 11c and ci), the binder amount increased. Consequently, the surface became smoother, and no evident voids was observed.

The microstructure analysis is consistent with the results from the density measurement and mechanical property characterization. An increase in the pressure from 0 MPa to 5 MPa led to a dramatic decrease in the porosity (Fig. 11g and h), which corresponds to a 7.3% increase in the density (Fig. 6b) and a $\sim\!302\%$ increase in the tensile strength (Fig. 9d). A lower porosity also contributed to an increase in the stiffness of the composite, including a $\sim\!623\%$ increase in the E-modulus (Fig. 9e) and a $\sim\!49\%$ decrease in the elongation (Fig. 9f). When the pressure further increased from 5 MPa to 10 MPa, the microstructure showed less evident difference leading to less dramatic change in the density and mechanical properties, as displayed in Fig. 9d-f. In comparison, the stepover did not affect the observable microstructure as significantly as the pressure, which explains the small decrease (i.e., 0.5–1.8%, Fig. 6b) in density when the step-over changed from 0.65 mm to 0.89 mm.

3.5. Burn rate

Printing parameters were found to significantly affect not only the burn rate but also burning surface evolution of the printed propellants (i. e., burning surface roughness). For a reliable, uniform thrust profile, locally, the burning surface should be uniform, perpendicular to the direction of burning. Such a burning surface was observed with a printed propellant with a homogeneous composition and low porosity (Fig. 12a). Some printed propellants produced non-uniform burning behavior which provided insight into how this printing method and range of printing parameters could be optimized for ideal burning behavior. Fig. 12b and c show two undesirable burning behaviors: a conical and tapered burning surface, respectively. The conical burning surface, or convective burning, was only seen from propellants that were highly saturated, i.e., binder was seen diffusing from the sample during printing, indicating stoichiometry and burning behavior that is similar to cast propellant. These propellant samples were not inhibited due to burning surface obscuration when inhibitor was used, therefore, this behavior could be due to standard convective burning. It could also suggest the potential existence of a radial concentration gradient of binder, where more binder was present at the periphery which resulted in a diffusion flame at the edges of the propellant that progresses down the sides of the propellant faster than in the center. The tapered surface may also be the result of a gradient in the binder concentration. The propellants were printed while laying on their side. As the binder was deposited, gravity forced the binder to migrate towards the bottom of the print, or one particular side of the propellant. As the propellant burned, the side with more binder tended to burn faster causing the tapered burning. This burning surface occurred particularly when the applied pressure was low and the step-over was small, which contributed to larger pores and thereby, lower capillary forces, allowing more binder to travel to the bottom layers with gravity. This indicates a threshold exists for the amount of binder which should be deposited for a given packing density. More research is needed to validate this hypothesis through carefully analyzing the spatial distribution of binder

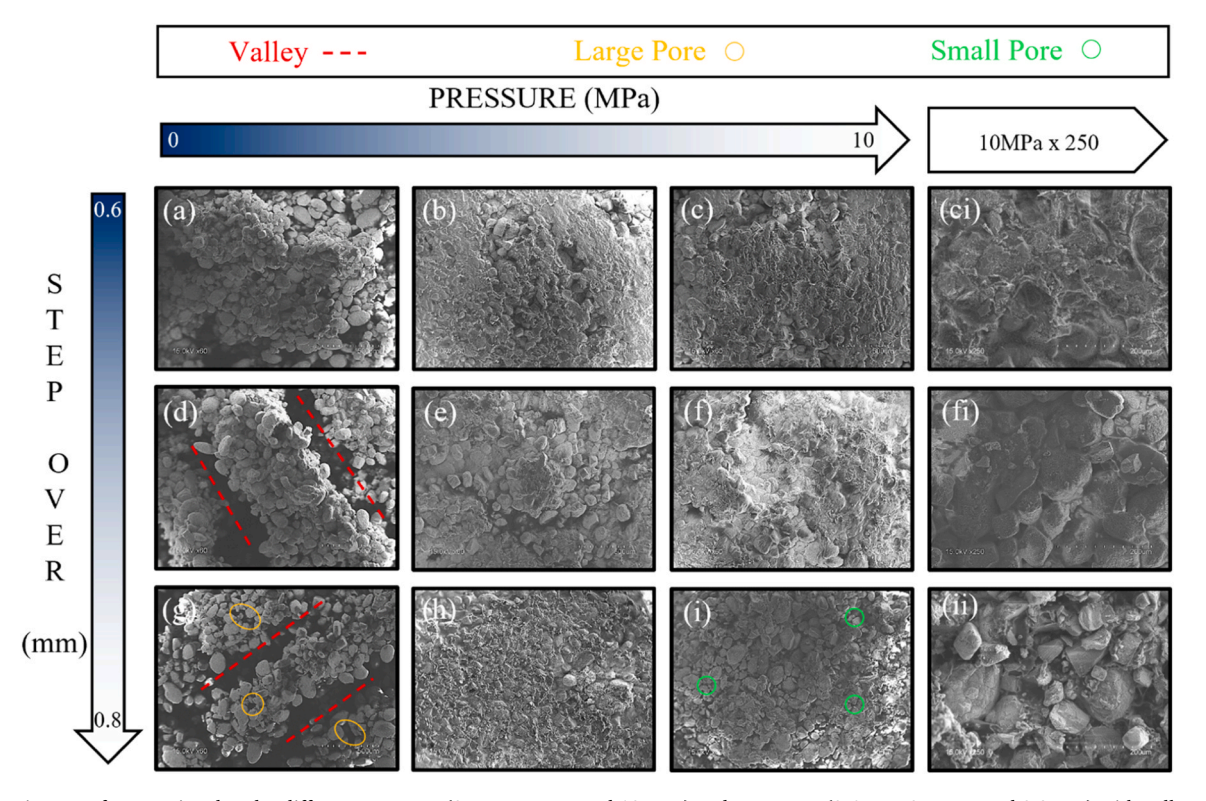


Fig. 11. SEM images of parts printed under different pressures (0 MPa, 5 MPa, and 10 MPa) and step-overs (0.6 mm, 0.7 mm, and 0.8 mm) with valleys and pores highlighted.

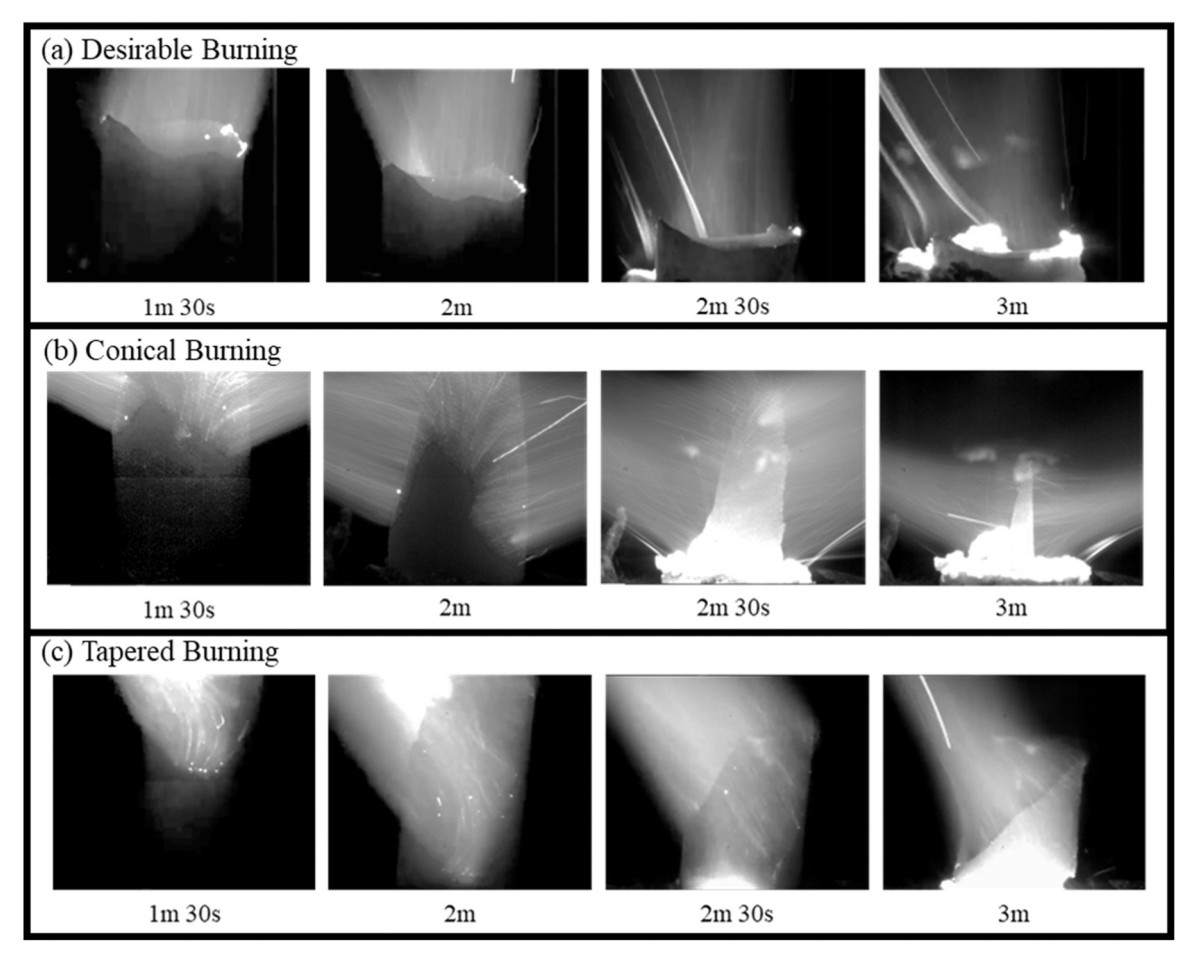


Fig. 12. Burning surfaces observed with the printed propellants, including (a) uniform, (b) conical, and (b) tapered.

within printed propellants, which will be the focus of our future study. Fig. 13 shows the effects of printing parameters on the burn rate. The propellant burning rate was found to be significantly affected by the applied pressure and step-over used in the fabrication. It should be noted that trials exhibiting the aforementioned behavior, i.e., undesirable burning surfaces, were not included in these reported burning rate results. The benchmark cast propellant in Fig. 13a was specifically created for this study using the same formulation as the printed samples, and its burning rate was experimentally determined using the same process/ setup. The propellants exhibited burn rates that were 15%, 25%, and 30% slower than that of the cast propellant for step-overs of 0.7 mm, 0.8 mm and 0.89 mm, respectively. A decrease in step-over was found to increase the burn rate (Fig. 13a). While at step-overs of 0.7 mm and larger, burn rate is relatively insensitive. When further reducing stepover from 0.7 mm to 0.65 mm, burning rate was approximately doubled and is also approximate twice the burning rate of the cast propellant. With the current knowledge, our hypothesis is that a smaller step-over resulted in more binder deposition, which allows for a fueloxidizer ratio closer to the stoichiometric ratio and consequently accelerates the burning rate of the propellant by providing additional energy and additional kinetic pathways for combustion [1].

Under varying applied pressures, it was found that the highest burn rate was produced when no pressure was applied (0.7 mm step-over), as displayed in Fig. 13b. As the applied pressure increased to 5–10 MPa, burning rates decreased by 25–37%. This is likely due to a tradeoff between porosity and binder content. With no applied pressure, the packing density of AP is lower, and the pores are filled with binder. This provides more binder as fuel for combustion at the burning surface resulting in faster burn rates. As pressure is applied, the packing density

of AP is increased, and the pore size is reduced. This reduces the binder ratio with respect to the sample volume and creates a more oxidizer-rich propellant with a reduced burning rate due to being farther from stoichiometry.

To demonstrate the capability of our process in tuning the properties of propellants in situ, dual-composition samples were printed by varying the step-over and applied pressure from one end to the other of a printed propellant strand (Fig. 13c). Three samples were made in total under the same processing conditions. For all the three samples, the top half was first printed with a step-over of 0.89 mm and a pressure of 5 MPa, while the bottom half was printed with a step-over of 0.65 mm and a pressure of 10 MPa. These parameters were chosen as they produced the slowest burn rates (top half of strand) and fastest burn rates (bottom half) in the previous trials and were the most likely to produce observable variation in burning rates, even over short distances. Fig. 13c and ci display the gradient samples in processing conditions as well as composition. Figure 13cii shows that the samples started off with a relatively slow burn rate for the "slow" half and then nearly doubled as the burning surface transitioned into the "fast" half. A clear transition point was found in the samples with a 90% change in the burn rate (i.e., the slope of the fitted lines), highlighting the feasibility of printing rate-tunable propellants with this method.

Propellants with various geometries were printed and ignited to demonstrate the geometry-dependent combustion surface evolution of the materials. The design and printing results are shown in Fig. 14a–c, including a spiral, a hollow-cored cylinder, and a dual spiral-cored cylinder. The evolution of burning is shown in Fig. 14. The combustion surface of the spiral propellant was able to follow the axial direction of the shape with classic end-burning while still maintaining a relatively

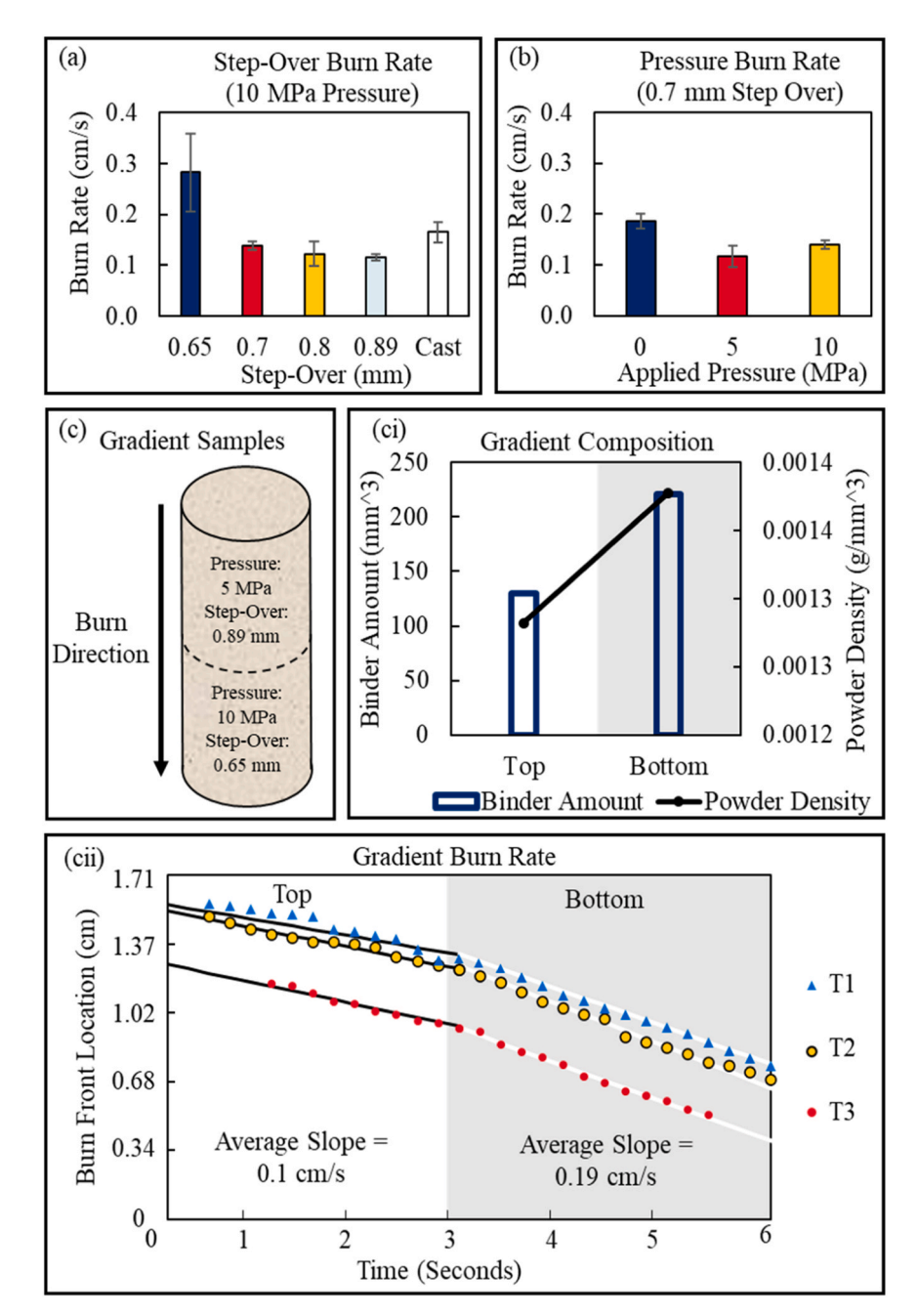


Fig. 13. Burn rates under different (a) step-overs with a constant pressure of 10 MPa and different (b) applied pressure with a constant step over distance of 0.7 mm; (c-ci) Functionally graded propellant composition and (cii) Burning surface position for three trials with functionally graded propellants printed by our PBJ process.

uniform burning surface. In comparison, the flame of the internal core features for both the single core and double-spiral core propagated down through the cores before propagating outward. There is, however, some deformation in the shape of final printed parts, which is visible in comparing 3D models to as-printed shapes in Fig. 14. Optimizing the shape would require adjustment of binder rheology and pressure. Regardless, the flexibility and precision of 3D printing such features may offer unique opportunities to create controllable and desirable convective burning for high-burn rate applications such as gun propellants [40, 41] and for developing novel, tailored thrust profiles.

Fig. 15 shows the pressurized burning of a printed propellant with a step-over of 0.89~mm and applied pressure of 10~MPa at a combustion pressure of 3.45~MPa. The specimen exhibited the desired burning behavior with a relatively flat burning surface. However, at burning pressures higher than 3.45~MPa, the samples displayed anomalous

burning behaviors with a high degree of burning surface variability and convective burning behavior. Such behavior at higher pressures indicates the presence of internal damage, such as voids, cracks, or debonding within the propellant [42], which likely stem from binder migration during printing. Future work will focus on investigating mitigation strategies for these issues. One potential route is through in situ curing of the binders during the printing of each layer, instead of post-print thermal cross-linking, as is done in this work. In addition, an AP powder formulation with a multi-modal size distribution could also be utilized to further improve the powder packing density.

4. Conclusion

Our PBJ process provides a unique, flexible, and effective method to fabricate tunable solid propellants with complex geometries. It paves an

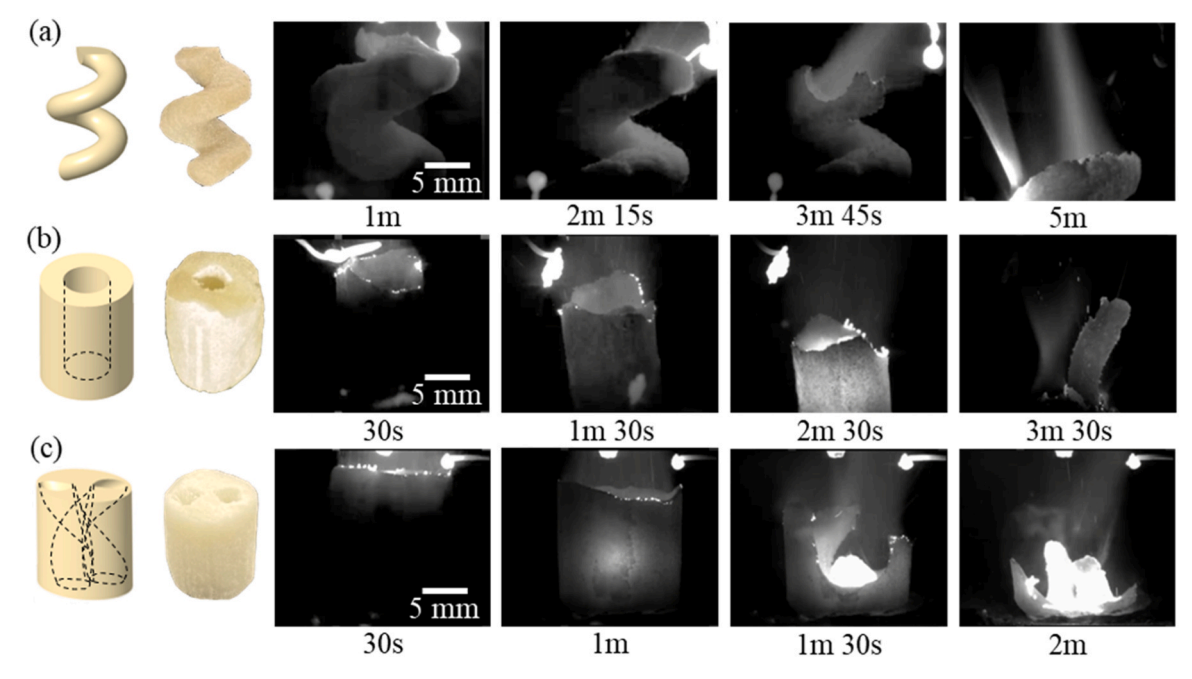


Fig. 14. Burning behavior for unique geometric propellants, including (a) a spiral, (b) a hollow-cored cylinder, and (c) a dual spiral-cored cylinder.

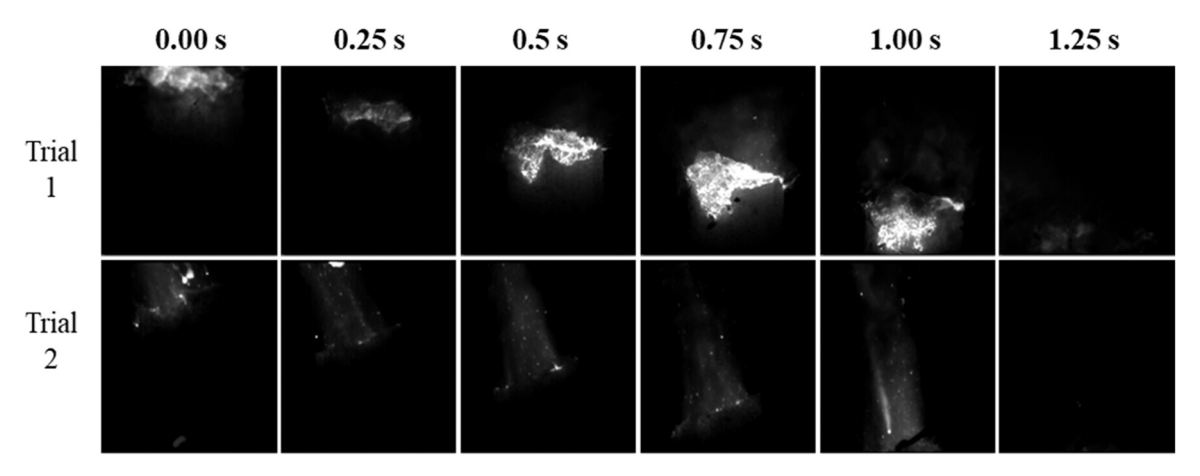


Fig. 15. Propellants burned at 3.45 MPa inside a nitrogen filled Crawford bomb. The printing step-over is 0.89 mm, and the printing pressure is 10 MPa.

avenue to fabricate solid propellants for mission-specific purposes while still maintaining similar mechanical strength and burning rates to traditional fabrication methods. Some key findings from this work are summarized as follows:

- (1) The PBJ process can achieve composite propellants with densities and solids loading comparable to or higher than those made by traditional methods (e.g., density ranging from 65% to 85.5% and solids loading ranging from 82.1% to 96.1%). The integrated pressing mechanism in PBJ can densify the powder bed with precise layerwise control; selective binder jetting allows lower binder concentrations to be selectively and precisely deposited within a composite, overcoming the limitations of existing AM processes in achieving high solids loading imposed by the feedstock flowability. Adjustment of the powder bed density and binder concentration provides a method to tune the density and solids loading of the propellant on a local scale within propellant articles. With fine tuning of the process and materials, PBJ shows great promise in the fabrication of highly dense propellants.
- (2) Mechanical properties and burning behaviors of PBJ-printed composite propellants are highly dependent on the processing
- parameters, including applied pressure and step-over. An increase in step-over resulted in a more elastic composite, whereas an increase in applied pressure caused the propellant to be stiffer. The tensile strength ranged from 0.11 to 0.88 MPa. E-modulus was in the range of 1.2-20.7 MPa. Elongation was able to reach a range of 4.1-9.1%. The uniformity of the burn was affected by binder saturation and binder migration in unsaturated propellants. With no pressure applied to the print bed, the burn rate was higher due to more binder content within the lower particle packing density. A higher applied pressure reduced the burning rate due to decreased binder content and a less balanced fuel-oxidizer ratio. A decrease in step-over provided more binder to the propellant and the additional fuel creates a more stoichiometric mixture, increasing the burn rate.
- (3) Altering the step-over alone can lead to a 90% change in burn rate. The layer-by-layer control of binder content, pressure, and binder distribution allow tailoring of burning rate in-situ within a printed propellant article. Preliminary results for pressurized burning exhibited fairly uniform burns at pressures lower than 3.45 MPa. However, a high degree of variability was found for pressures above 3.45 MPa and future efforts should investigate

- methods for mitigating any internal damage that could cause this behavior.
- (4) Further research efforts can be directed towards examining the spatial distribution and chemistry of the binder within solid propellants fabricated using the PBJ technique, along with their consequential impacts on burning behaviors. Future work can also involve the optimization of material and process to enhance the printing resolution. Additionally, more investigations can be conducted to enable new binder formulations suitable for inkjetting. These formulations should avoid the incorporation of evaporative diluents that could introduce pores during evaporation.

CRediT authorship contribution statement

Kirby Levi: Writing – review & editing, Writing – original draft, Visualization, Validation, Methodology, Investigation. Lawrence Adam: Writing – review & editing, Visualization, Validation, Methodology, Investigation. Udaykumar H.S.: Writing – review & editing, Funding acquisition, Conceptualization. Sippel Travis: Writing – review & editing, Funding acquisition, Conceptualization. Song Xuan: Writing – review & editing, Writing – original draft, Supervision, Investigation, Funding acquisition, Conceptualization.

Declaration of Competing Interest

The authors declare the following financial interests/personal relationships which may be considered as potential competing interests: Xuan Song reports financial support was provided by Air Force Office of Scientific Research. Xuan Song reports financial support was provided by National Science Foundation. Travis Sippel reports financial support was provided by Air Force Office of Scientific Research. H.S. Udaykumar reports financial support was provided by National Science Foundation. H.S. Udaykumar reports financial support was provided by Air Force Office of Scientific Research.

Data availability

Data will be made available on request.

Acknowledgements

The authors would like to acknowledge the support from the U.S. Air Force Office of Scientific Research under grant number FA9550–20-1–0700 (Program Officer: Martin Schmidt and Chiping Li). H.S.U. and X. S. would also like to acknowledge the support from the U.S. National Science Foundation under grant number 2118393.

References

- M.W. Beckstead, Recent progress in modeling solid propellant combustion, Combustion, Explosion, Shock Waves 42 (6) (2006) 623–641.
- [2] W.M. Adel, L. Guo-Zhu, Analysis of mechanical properties for AP/HTPB solid propellant under different loading conditions, Int. J. Aerosp. Mech. Eng. 11 (12) (2017) 1915–1919.
- [3] M. McClain, I. Gunduz, S. Son, Additive manufacturing of ammonium perchlorate composite propellant with high solids loadings, Proc. Combust. Inst. 37 (3) (2019) 3135–3142.
- [4] R.A. Chandru, N. Balasubramanian, C. Oommen, B. Raghunandan, Additive manufacturing of solid rocket propellant grains, J. Propuls. Power 34 (4) (2018) 1090–1093.
- [5] S. Chaturvedi, P.N. Dave, Solid propellants: AP/HTPB composite propellants, Arab. J. Chem. 12 (8) (2019) 2061–2068.
- [6] J. van Lingen, Gradient Additive Manufacturing of Energetics Research (GAMER), Neth. Organ. Appl. Sci. Res. (2022).
- [7] W. Dunju, G. Changping, W. Ruihao, Z. Baohui, G. Bing, N. Fude, Additive manufacturing and combustion performance of CL-20 composites, J. Mater. Sci. 55 (7) (2020) 2836–2845.
- [8] M.S. McClain, A. Afriat, J.F. Rhoads, I.E. Gunduz, S.F. Son, Development and characterization of a photopolymeric binder for additively manufactured

- composite solid propellant using vibration assisted printing, Propellants, Explos., Pyrotech. 45 (6) (2020) 853–863.
- [9] K. Nagendra, C. Vijay, P. Ramakrishna, Binder melt: Quantification using SEM/EDS and its effects on composite solid propellant combustion, Proc. Combust. Inst. 37 (3) (2019) 3151–3158.
- [10] I. Gunduz, M. McClain, P. Cattani, G.-C. Chiu, J. Rhoads, S.J.Am Son, 3D printing of extremely viscous materials using ultrasonic vibrations, 22, 2018: 98–103.
- [11] M.S. McClain, A. Afriat, B.J. Montano, J.F. Rhoads, I.E. Gunduz, S.F. Son, Dynamic combustion of functionally graded additively manufactured composite solid propellant, J. Propuls. Power. 37 (5) (2021) 725–732.
- [12] M. Li, W. Yang, M. Xu, R. Hu, L. Zheng, Study of photocurable energetic resin based propellants fabricated by 3D printing, Mater. Des. 207 (2021), 109891.
- [13] W. Yang, R. Hu, L. Zheng, G. Yan, W. Yan, Fabrication and investigation of 3D-printed gun propellants, Mater. Des. 192 (2020), 108761.
- [14] S. Garino, P. Antonaci, D. Pastrone, M. Sangermano, F. Maggi, Photopolymerization for additive manufacturing of composite solid propellants, Acta Astronaut. 182 (2021) 58–65.
- [15] N.V. Muravyev, K.A. Monogarov, U. Schaller, I.V. Fomenkov, A.N.J.P. Pivkina, Explosives, Pyrotechnics, Progress in additive manufacturing of energetic materials: Creating the reactive microstructures with high potential of applications, 44(8), 2019: 941–969.
- [16] R. Kurva, S. Ukey, M. Modgi, Experimental Approaches to Develop a High Thrust Ratio in a Single Chamber Dual Thrust Motor Using a Composite Propellant Formulation Based on HTPB/AP/Al, Central European, J. Energ. Mater. 14 (4) (2017)
- [17] A. Aziz, R. Mamat, W.K. Wan Ali, M.R. Mohd, Perang, Review on typical ingredients for ammonium perchlorate based solid propellant, Applied Mechanics and Materials, Trans. Tech. Publ. (2015) 470–475.
- [18] H. Naseem, J. Yerra, H. Murthy, P. Ramakrishna, Ageing studies on AP/HTPB based composites solid propellants, Energ. Mater. Front. 2 (2) (2021) 111–124.
- [19] N. Eisenreich, T.S. Fischer, G. Langer, S. Kelzenberg, V. Weiser, Burn rate models for gun propellants, Propellants, Explosives, Pyrotechnics, Int. J. Deal. Sci. Technol. Asp. Energ. Mater. 27 (3) (2002) 142–149.
- [20] T. Sippel, J. Michael, S. Barkley, K. Zhu, I.S.U.A.U. States, Pulsed microwave plasma instrumentation for investigation of plasma-tuned multiphase combustion, Final Report, DISTRIBUTION A: Distribution Approved for Public Release, 2018.
- [21] S. Barkley, K. Zhu, J. Lynch, M. Ballestero, J. Michael, T.R. Sippel, Microwavesupported plasma combustion enhancement of composite solid propellants using alkali metal dopants, 54th AIAA Aerospace Sciences Meeting, 2016, p. 0685.
- [22] K. Zhu, S.J. Barkley, T.R. Sippel, J.B. Michael, Emission thermometry of microwave-assisted alkali-doped propellant combustion, Combust. Flame 251 (2023), 112704.
- [23] N.P. Rao, C. Solanke, B.K. Bihari, P.P. Singh, B.J.P. Bhattacharya, Explosives, Pyrotechnics, Evaluation of mechanical properties of solid propellants in rocket motors by indentation technique, 41(2), 2016: 281–285.
- [24] F. Fei, L. He, L. Kirby, X. Song, Study of droplet diffusion in hydrothermal-assisted transient jet fusion of ceramics, J. Manuf. Sci. Eng. 143 (5) (2021), 051001.
- [25] F. Fei, L. Kirby, X. Song, Process Optimization for Hydrothermal-Assisted Jet Fusion Additive Manufacturing of Ceramics, International Manufacturing Science and Engineering Conference, American Society of Mechanical Engineers, 2022, p. V001T01A037
- [26] M. Zebregs, A.E. Mayer, A.E. van der Heijden, Comparison of propellant processing by cast-cure and resonant acoustic mixing, Propellants, Explos., Pyrotech. 45 (1) (2020) 87–91.
- [27] C. Brown, Experimental characterization and numerical modeling of additivemanufactured composite solid rocket propellant with anisotropic density, Colo. Sch. Mines (2019).
- [28] D.C. Purcell, An Analysis, of Optimizing Properties of Solid Rocket Propellant for 3-D Printing, N. Mex. Inst. Min. Technol. (2022).
- [29] S. Park, S. Choi, K. Kim, W. Kim, J. Park, Effects of Ammonium Perchlorate Particle Size, Ratio, and Total Contents on the Properties of a Composite Solid Propellant, Propellants, Explos., Pyrotech. 45 (9) (2020) 1376–1381.
- [30] K.S. Babu, P.K. Raju, C. Thomas, A.S. Hamed, K. Ninan, Studies on composite solid propellant with tri-modal ammonium perchlorate containing an ultrafine fraction, Def. Technol. 13 (4) (2017) 239–245.
- [31] R. Sangtyani, A. Kumar, M. Gupta, Optimization of network forming agents for different types of composite propellant grain, Cent, Eur. J. Energetic Mater. 10 (3) (2013)
- [32] H. Shekhar, D.K. Kankane, Viscoelastic characterization of different solid rocket propellants using the Maxwell spring-dashpot model, Cent. Eur. J. Energetic Mater. 9 (3) (2012) 189–199.
- [33] Y. Jiao, S. Li, S. Ding, D. Yang, C. Bai, J. Liu, Y. Luo, G. Li, Preparation and Properties of Nitrocellulose/Viton Based Nano Energetic by Direct Writing, 2021 International Conference on Development and Application of Carbon Nanomaterials in Energetic Materials, Springer, 2022, pp. 341–352.
- [34] B.C.C. Da Cunha, E. da Costa Mattos, J.A.F.F. Rocco, Influence of storage time before casting on viscosities and mechanical properties of AP/HTPB/Al solid composite propellants, FirePhysChem. 2 (1) (2022) 50–55.
- [35] S. Nandagopal, M. Mehilal, M. Tapaswi, S. Jawalkar, K. Radhakrishnan, B.J.P. Bhattacharya, Explosives, Pyrotechnics: An International Journal Dealing with Scientific, T.A.o.E. Materials, Effect of coating of ammonium perchlorate with fluorocarbon on ballistic and sensitivity properties of AP/Al/HTPB propellant, 34 (6), 2009: 526–531.
- [36] A.T. Kebede, E. Balasubramanian, A. Praveen, L. Rohit, K. Arvind, Preliminary investigations on extrusion of high viscosity slurry using direct writing technique, Int. J. Simul. Multidiscip. Des. Optim. 11 (2020) 15.

- [37] N.P. Rao, C. Solanke, B.K. Bihari, P.P. Singh, B. Bhattacharya, Evaluation of mechanical properties of solid propellants in rocket motors by indentation technique, Propellants, Explos., Pyrotech. 41 (2) (2016) 281–285.
- [38] J.C. Thomas, A.R. Demko, T.E. Sammet, D.L. Reid, S. Seal, E.L. Petersen, Mechanical properties of composite AP/HTPB propellants containing novel titania nanoparticles, Propellants, Explos., Pyrotech. 41 (5) (2016) 822–834.
- [39] K. Ramesh, S.N. Jawalkar, S. Sachdeva, B. Bhattacharya, Development of a composite propellant formulation with a high performance index using a pressure casting technique, Central Eur. J. Energ. Mater. 9 (1) (2012) 49–58.
- [40] B. Ermolaev, A. Sulimov, A. Roman'kov, V. Khrapovskii, A. Belyaev, A. Crowley, Convective burning of block charges prepared from seven-perforation propellant powder grains inhibited by polyvinyl butyral, Russ. J. Phys. Chem. B 9 (3) (2015) 375–384.
- [41] V. Khrapovskii, V. Khudaverdiev, Onset and development of convective burning in highly porous charges of ammonium perchlorate and its mixtures with aluminum, Russ. J. Phys. Chem. B 4 (1) (2010) 53–62.
- [42] T. Godai, Flame propagation into the crack of solid-propellant grain, AIAA J. 8 (7) (1970) 1322–1327.